

# Numerical tool to take nonlocal effects into account in metallo-dielectric multilayers

JESSICA BENEDICTO,<sup>1,2</sup> RÉMI POLLÈS,<sup>1,2</sup> CRISTIAN CIRACÌ,<sup>3</sup> EMMANUEL CENTENO,<sup>1,2</sup>  
DAVID R. SMITH,<sup>4</sup> AND ANTOINE MOREAU<sup>1,2,4,\*</sup>

<sup>1</sup>Clermont Université, Université Blaise Pascal, Institut Pascal, BP 10448, F-63000 Clermont-Ferrand, France

<sup>2</sup>CNRS, UMR 6602, IP, F-63171 Aubière, France

<sup>3</sup>Istituto Italiano di Tecnologia (IIT), Center for Biomolecular Nanotechnologies, Via Barsanti, I-73010 Arnesano, Italy

<sup>4</sup>Center for Metamaterials and Integrated Plasmonics, Duke University, Durham, North Carolina 27708, USA

\*Corresponding author: antoine.moreau@univ-bpclermont.fr

Received 23 April 2015; revised 6 July 2015; accepted 12 July 2015; posted 14 July 2015 (Doc. ID 239694); published 31 July 2015

We provide a numerical tool to quantitatively study the impact of nonlocality arising from free electrons in metals on the optical properties of metallo-dielectric multilayers. We found that scattering matrices are particularly well suited to take into account the electron response through the application of the hydrodynamic model. Though effects due to nonlocality are, in general, quite small, they, nevertheless, can be important for very thin (typically below 10 nm) metallic layers, as in those used in structures characterized by exotic dispersion curves. Such structures include those with a negative refractive index, hyperbolic metamaterials, and near-zero index materials. Higher wave vectors mean larger nonlocal effects, so that it is not surprising that subwavelength imaging capabilities of hyperbolic metamaterials are found to be sensitive to nonlocal effects. We find in all cases that the inclusion of nonlocal effects leads to at least a 5% higher transmission through the considered structure. © 2015

Optical Society of America

**OCIS codes:** (260.3910) Metal optics; (230.4170) Multilayers; (160.3918) Metamaterials.

<http://dx.doi.org/10.1364/JOSAA.32.001581>

## 1. INTRODUCTION

Metallo-dielectric multilayers [1] are a class of metamaterials that have attracted considerable attention because they are relatively easy to fabricate at infrared and visible wavelengths, and can support a wide scope of exotic behavior, including negative refraction and hyperbolic dispersion [2–8]. The unique properties of these multilayer structures can potentially play a role in applications, such as thermal radiation control [9–11] and subwavelength imaging [2,5,12–19]. To date, most of the analyses assume the local approximation for the electron response of the metal. However, as the metal layers become very thin and are closely spaced together, it can be expected that the local response model will no longer be applicable, and must be substituted with a nonlocal or full quantum mechanical model. Recent experiments [20] have indicated that there may be a length scale where the local approximation fails, but where the semiclassical, hydrodynamic model [21,22] for the free electron response is valid. The hydrodynamic model, while considerably approximate with respect to a full-quantum treatment, provides a more tractable model for analytic and semi-analytic calculations, especially for larger structures, and, thus, is an attractive approach for estimating the impact of nonlocality in various scenarios.

Over the last few years, there have been diverging opinions as to whether structures composed of very thin metallic and dielectric layers are sensitive to the intrinsic nonlocality of metals [23–25]. Hoping to help tackle this problem, we provide numerical tools to take into account nonlocal effects when calculating optical properties of any kind of metallo-dielectric multilayer. Our description relies on the hydrodynamic model [21,22], which has been shown to provide quantitative agreement for the plasmon resonance shifts observed on a system of gold nanospheres placed at sub-nanometer distances from a gold film [20]. This model was subsequently modified to take into account interband transitions [26].

In this paper, we present a scattering matrix formalism for metallo-dielectric multilayers, incorporating the effects of nonlocality through the use of the hydrodynamic model. Our formalism makes it easy to choose different boundary conditions [26], and, hence, to retrieve all previous models [25,27,28] that neglect interband transitions. Using these tools, we show that the impact of nonlocality on a recently published optical negative index ( $n = -1$ ) lens design based on metallo-dielectric multilayers [8] can be observed, although very moderate. By contrast, we find that nonlocal effects cannot be neglected for structures in the canalization (or channeling) regime [13]; moreover, for very

thin metallic layers, the bulk plasmon acts like a supplementary energy channel, allowing light to tunnel through metallic layers.

## 2. HYDRODYNAMICAL MODEL FRAMEWORK

Within the framework of the hydrodynamical model, conduction electrons are treated as gas constrained within the boundaries of the metal structure. Interactions between electrons are taken into account in an approximate manner through the introduction of a pressure term that includes the quantum pressure. The hydrodynamical equations are linearized [29] to yield a relation between the electric field and the polarization of the metal linked to the free electron displacements. The inclusion of the pressure terms in the hydrodynamic equations introduces a spatial derivative into the linearized equation of motion, and the response of the electron gas is, thus, nonlocal [30].

The origin of the hydrodynamic model can be traced to the physics of plasmas. It has been used to describe metallic structures since the 1960s and onward [31,32], raising many questions along the way as to the proper treatment of a metal-dielectric interface. Thus, the model suffered from many uncertainties, but was nonetheless widely used [33–36] and discussed [21,22,37]; then it was somewhat abandoned, likely because of the lack of any clear experimental evidence for nonlocal effects. It is clear now, for instance, that nonlocality has almost no impact on the surface plasmons of a thin metal film [26], although the shift in the plasmon resonance wavelength of prism-coupled films was often considered as a test for nonlocal theories [22].

A variety of other approaches has been proposed to take nonlocality into account, including the classical Random Phase Approximation [31,34,38,39] or Feibelman's model [40,41]. It is interesting to note that an essential improvement to the latter approach concerns the manner in which the contribution from bound electrons is taken into account [42]. However, this model is known for not having issues to take bulk absorption into account [39].

More modern approaches to assessing the electron response rely on the density functional theory (DFT), considered one of the most accurate tools to incorporate the effects of quantum mechanical interactions on resonances and other properties of metallic nanoparticles and nanoclusters [43,44]. These methods, while being very accurate, cannot be applied to systems that exceed a few thousands of electrons. As a consequence, the propagation of waves is usually not taken directly into account [45], which may be a problem for structures supporting gap plasmons and similarly confined modes.

The hydrodynamical model has attracted increasing attention because of advances in nanofabrication and measurement techniques that allow structures to be designed and studied in the regime where nonlocal response is expected to dominate [46–48]. In general, the hydrodynamic model is attractive because (1) its predictions are in good agreement with experiments for which nonlocality clearly plays a role [20], and well before other quantum effects kick in [49,50]; (2) it yields analytical results [26,51] and provides deeper insight into the physics of nonlocality; and (3) it is easy to implement in numerical simulations [52]. In addition, the uncertainties about the boundary conditions are lifted when the contribution of the bound

and free electrons are clearly distinguished [26] and its well-known tendency to overestimate the impact of nonlocality is lessened. This is especially relevant for very short wavelengths, when the permittivity is small and when the Drude term is of the order of the interband transition contribution. Thus, for the reasons above, the model has been used to study the enhancement by plasmonics tips [53] and dimers [54], hyperbolic metamaterials [25,28], subwavelength imaging by a silver slab [23,48], and gap plasmon propagation [26,48,55].

Finally, it should be stressed that, even if the model was found to be quite accurate [24] when compared to other approaches, it still has to be backed by more fundamental studies [44], comparisons to experiments [56], or even more sophisticated hydrodynamic models [30].

We will in this section briefly remind the reader of the fundamental physics of nonlocality within the framework of the hydrodynamical model when the contribution of bound electrons is taken into account. A detailed derivation of these equations can be found in [26].

### A. Longitudinal Waves

Let us consider a multilayer as represented in Fig. 1. Nonlocal effects are expected to occur for *p*-polarization only (sometimes referred to as TM), so that we will from now on consider this polarization only. We assume the structure is illuminated with a plane wave characterized by the angular frequency  $\omega$  (time dependency  $e^{-i\omega t}$ ) and a wave vector whose component along the *x* axis is denoted  $k_x$ .

In the framework of the hydrodynamic model [46,57], the electric and magnetic fields satisfy Maxwell's equations:

$$\nabla \times \mathbf{E} = i\omega\mu_0\mathbf{H}, \quad (1)$$

$$\nabla \times \mathbf{H} = -i\omega\epsilon_0(1 + \chi_b)\mathbf{E} + \mathbf{P}_f, \quad (2)$$

where the effective polarization of the medium is linked to the electric field by the fundamental relation [26]

$$\mathbf{P}_f = \frac{\epsilon_0 \cdot \omega_p^2}{\omega^2 + i\gamma\omega} \left( \mathbf{E} - (1 + \chi_b) \frac{\beta^2}{\omega_p^2} \nabla(\nabla \cdot \mathbf{E}) \right). \quad (3)$$

These equations can be easily solved to yield an analytical form for the fields.

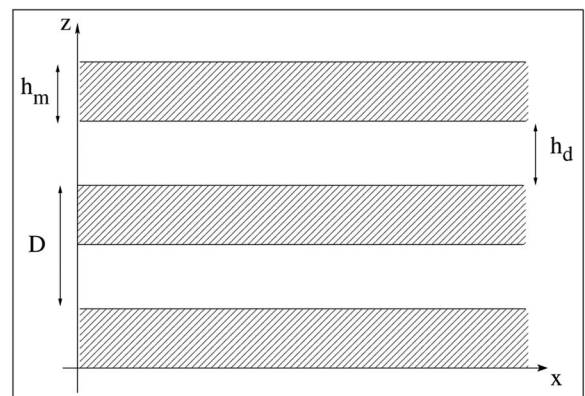


**Fig. 1.** Diagram of an infinitely periodic metallo-dielectric structure. The gray areas represent the metallic layers.

In the  $j$ -th dielectric layer, having a relative permittivity  $\epsilon_d$ , the magnetic and electric fields can be written

$$H_{y_d} = (A_j e^{ik_d z} + B_j e^{-ik_d z}) e^{i(k_x x - \omega t)}, \quad (4)$$

$$E_x = \frac{k_d}{\omega \epsilon_0 \epsilon_d} (A_j e^{ik_d z} - B_j e^{-ik_d z}) e^{i(k_x x - \omega t)}, \quad (5)$$

$$E_z = \frac{-k_x}{\omega \epsilon_0 \epsilon_d} (A_j e^{ik_d z} + B_j e^{-ik_d z}) e^{i(k_x x - \omega t)}, \quad (6)$$

with  $k_d = \sqrt{\epsilon_d k_0^2 - k_x^2}$  and  $k_0 = \frac{\omega}{c}$ . We choose the branch cut for the square root to be on the negative imaginary axis [58]. This peculiar choice guarantees that the imaginary part of the square root is positive. While this has no impact on the following analytical calculations, such a choice is critical for the numerical stability of the method as explained in [59].

Inside the  $j$ -th metallic layer of permittivity  $\epsilon_m$  in the framework of the hydrodynamical model, two types of waves are supported: the transverse, for which  $\nabla \cdot \mathbf{E} = 0$ , and the longitudinal waves for which  $\nabla \times \mathbf{E} = \mathbf{0}$ , and, consequently,  $\mathbf{H} = \mathbf{0}$ . The transverse wave solutions can be found from the consideration of the two Maxwell curl equations: if  $\nabla \cdot \mathbf{E} = 0$ ,  $\mathbf{P}_f = \mathbf{0}$  and equations Eqs. (1) and (2) reduce to the usual, local, curl equations:

$$\partial_z E_x - \partial_x E_z = i\omega \mu_0 H_y, \quad (7)$$

$$E_x = \frac{1}{i\omega \epsilon_0 \epsilon_m} \partial_z H_y, \quad (8)$$

$$E_z = -\frac{1}{i\omega \epsilon_0 \epsilon_m} \partial_x H_y, \quad (9)$$

so that, inside the metal, they can be written

$$H_{y_m} = (A_j e^{-\kappa_t z} + B_j e^{\kappa_t z}) e^{i(k_x x - \omega t)}, \quad (10)$$

$$E_x^t = \frac{i\kappa_t}{\omega \epsilon_0 \epsilon_m} (A_j e^{-\kappa_t z} - B_j e^{\kappa_t z}) e^{i(k_x x - \omega t)}, \quad (11)$$

$$E_z^t = \frac{-k_x}{\omega \epsilon_0 \epsilon_m} (A_j e^{-\kappa_t z} + B_j e^{\kappa_t z}) e^{i(k_x x - \omega t)}, \quad (12)$$

where  $\kappa_t = \sqrt{k_x^2 - \epsilon_m k_0^2}$ . The branch cut in that case must be chosen on the negative real axis for numerical stability. This is important here, as  $\epsilon_m$  usually presents an important imaginary part [60]. The longitudinal wave corresponds to a bulk plasmon supported by the free electron gas, with no accompanying magnetic field. Because the electric field corresponding to the longitudinal mode is thus curl free, it satisfies

$$\partial_z E_x = \partial_x E_z, \quad (13)$$

and, finally, can be written (the first equation below being the definition of  $C_j$  and  $D_j$ )

$$E_x^\ell = \frac{1}{\omega \epsilon_0} (C_j e^{-\kappa_\ell z} + D_j e^{\kappa_\ell z}) e^{i(k_x x - \omega t)}, \quad (14)$$

$$E_z^\ell = \frac{-\kappa_\ell}{ik_x \omega \epsilon_0} (C_j e^{-\kappa_\ell z} - D_j e^{\kappa_\ell z}) e^{i(k_x x - \omega t)}, \quad (15)$$

with

$$\kappa_\ell = \sqrt{k_x^2 + \frac{\omega_p^2}{\beta^2} \left( \frac{1}{\chi_f} + \frac{1}{1 + \chi_b} \right)}, \quad (16)$$

where  $\omega_p$  is the plasma frequency of the considered metal, and  $\chi_f$  and  $\chi_b$  are the susceptibilities associated with the free and bound electrons, respectively ( $\epsilon_m = 1 + \chi_b + \chi_f$ ). These three parameters are determined through careful fits of the metal permittivity [60]. The data on which these fits rely are obtained in situations where nonlocality plays no role, and clearly distinguish the free electron response from the interband transitions in the framework of an intrinsically local description. Then nonlocality can be taken into account through the parameter  $\beta$ , which is, however, not so easy to estimate. This constant can account for both Coulomb interaction and quantum pressure through which free electrons interact strongly in the metal [29,30], and is proportional to the Fermi velocity, even if the theoretical value of the proportionality coefficient depends on the model that is chosen. The recent experimental results on film-coupled nanoparticles show that a value somewhat smaller than the Fermi velocity is a good estimate. Since gold and silver present very close Fermi velocities, we take here  $\beta = 1.35 \times 10^6$  m/s for both metals [20,46].

## B. Additional Boundary Conditions

At the boundary between a metal and a dielectric, an additional boundary condition is needed to determine to what extent the longitudinal wave is excited. Many different boundary conditions have been used in the past, but it becomes more and more widespread to use the fact that the normal component of the current should be continuous, as very clearly discussed elsewhere [28]. This leads us to write here that, at the interface between a metal and a dielectric, the normal polarization has to vanish:  $P_{fz} = 0$ , since  $i\omega \mathbf{P} = \mathbf{j}$  [29]. This is imposed by the conservation of charges and seems to be the only physical choice when the contribution of the bound electrons is distinguished from the response of the free ones [26]. This distinction is pointless in the case of the Drude model, but crucial when studying nonlocality; it can be done accurately when based on extensive data and careful fits [60]. Separating the different contributions, but using a less physical boundary condition [51,53], can lead to an exaggeration of the nonlocal effects [26]. We emphasize that this combination of a clear separation between the different electronic responses and the use of the boundary conditions that physically derive from this choice, to the best of our knowledge, has never been done in previous works on multilayers [25,27,28,61].

For the fields that are inside the metal, the boundary condition on the polarization can be written on the interface:

$$P_{fz} = -\frac{1}{i\omega} \partial_x H_y - \epsilon_0 (1 + \chi_b) E_z = 0, \quad (17)$$

where, of course,  $\mathbf{E} = \mathbf{E}^t + \mathbf{E}^\ell$ . Using Eq. (9), the previous condition can also be written

$$E_z^\ell = \frac{\kappa_\ell}{\omega \epsilon_0 k_x} \Omega H_y, \quad (18)$$

with

$$\Omega = \frac{k_x^2}{\kappa_l} \left( \frac{1}{\epsilon} - \frac{1}{1 + \chi_b} \right). \quad (19)$$

Considering different boundary conditions, as done elsewhere, would only lead to slightly different expressions for  $\kappa_l$  and  $\Omega$  [26].

### 3. SCATTERING MATRIX ALGORITHM

Metallo-dielectric multilayers are of heightened interest in many metamaterial configurations for their unique dispersion characteristics. While a fully isotropic negative index and other novel metamaterial media are difficult to realize at visible and infrared wavelengths, anisotropic media composing alternating metal/dielectric layers can be readily fabricated and can often approximate the desired wave propagation effects. In particular, one striking property that can be achieved in metallo-dielectric multilayers is hyperbolic dispersion [62,63]. Hyperbolic metamaterials are compelling because the hyperbolic dispersion relation allows evanescent waves emitted by a source to be converted to propagating waves. This effect can be used to achieve subwavelength imaging [13,15,18,19,64,65], projection of near-field information to far-field [5,14], and super-Planckian thermal emission [9,11]. The dispersion relation for infinitely periodic metallo-dielectric multilayers [27,61] makes it possible to retrieve very important parameters, such as the effective index of the structure [19]. It is, however, not sufficient, because it does not give any information on the reflection coefficients on the structure for the incoming field, or inside the structure for the Bloch modes. We underline that, even for structures with simple patterns, the first and the last layer are usually made of the same material, thus limiting the insight the dispersion relation can provide; it does not give access to the reflection coefficient [25]. Furthermore, more complex patterns have recently attracted a lot of attention [8,66], for which the dispersion relation has no analytical expression. For these reasons, a systematic way for calculating the reflection coefficient of a metallo-dielectric structure and the field inside any layer is required. This is all the more reason that cavity resonances in metallo-dielectric layers [67] may complicate the global picture given by the dispersion curves.

A transfer matrix method was proposed in the 1980s [27], but it is not simple to use. As a dielectric and a metallic layer lead to transfer matrices with different sizes, they cannot simply be multiplied, so that this technique has been used to study infinite multilayers of two different nonlocal metals [61]. In addition, transfer matrices are not expected to be numerically stable for metallo-dielectric multilayers below the plasma frequency when the waves are evanescent [59]. As we will see in this section, the scattering matrices are an elegant way to take nonlocality into account, because they can be combined very easily. In addition, they are numerically perfectly stable so that they constitute a natural choice. Our method has been validated by comparison with full Comsol [68] simulations, in which a customized implementation of the full hydrodynamic equation was included [46,69].

#### A. Layer Matrices

Let us consider a layer  $j$  whose interfaces are located at  $z = z_j$  and  $z = z_{j+1}$ . The thickness of the layer is  $h_j = z_j - z_{j+1}$ . It is

convenient to introduce here the coefficients  $A_j^\pm$  and  $B_j^\pm$ , which are defined in a dielectric layer by

$$H_y = (A_j^+ e^{ik_z^j(z-z_j)} + B_j^+ e^{-ik_z^j(z-z_j)}) e^{i(k_x x - \omega t)}, \quad (20)$$

$$= (A_j^- e^{ik_z^j(z-z_{j+1})} + B_j^- e^{-ik_z^j(z-z_{j+1})}) e^{i(k_x x - \omega t)}, \quad (21)$$

with  $k_z^j = \sqrt{\epsilon_j k_0^2 - k_x^2}$ ,  $\epsilon_j$  being the relative permittivity of the dielectric medium. Using Maxwell's equations for  $p$ -polarization Eq. (9), the electric field ( $E_x$ ,  $E_z$ ) can be calculated easily.

This leads to introducing a scattering matrix for a dielectric layer that is written

$$\begin{bmatrix} A_j^+ \\ B_j^- \end{bmatrix} = \begin{bmatrix} 0 & e^{ik_z^j h_j} \\ e^{ik_z^j h_j} & 0 \end{bmatrix} \begin{bmatrix} B_j^+ \\ A_j^- \end{bmatrix}. \quad (22)$$

Inside a metallic layer, coefficients can be defined similarly for the transversal wave as

$$H_y = (A_j^+ e^{-\kappa_l(z-z_j)} + B_j^+ e^{\kappa_l(z-z_j)}) e^{i(k_x x - \omega t)}, \quad (23)$$

$$= (A_j^- e^{-\kappa_l(z-z_{j+1})} + B_j^- e^{\kappa_l(z-z_{j+1})}) e^{i(k_x x - \omega t)}, \quad (24)$$

and the corresponding electric field can be determined using Eq. (9). Taking the longitudinal wave into account leads to introducing coefficients  $C_j^\pm$  and  $D_j^\pm$ :

$$E_x^\ell = \frac{1}{\omega \epsilon_0} (C_j^+ e^{-\kappa_l(z-z_j)} + D_j^+ e^{\kappa_l(z-z_j)}) e^{i(k_x x - \omega t)}, \quad (25)$$

$$= \frac{1}{\omega \epsilon_0} (C_j^- e^{-\kappa_l(z-z_{j+1})} + D_j^- e^{\kappa_l(z-z_{j+1})}) e^{i(k_x x - \omega t)}. \quad (26)$$

This leads to a scattering matrix for a metallic layer that is written

$$\begin{bmatrix} A_j^+ \\ C_j^+ \\ B_j^- \\ D_j^- \end{bmatrix} = \begin{bmatrix} 0 & 0 & e^{-\kappa_l h_j} & 0 \\ 0 & 0 & 0 & e^{-\kappa_l h_j} \\ e^{-\kappa_l h_j} & 0 & 0 & 0 \\ 0 & e^{-\kappa_l h_j} & 0 & 0 \end{bmatrix} \begin{bmatrix} B_j^+ \\ D_j^+ \\ A_j^- \\ C_j^- \end{bmatrix}. \quad (27)$$

#### B. Dielectric to Metal Scattering Matrix

We assume here that medium  $j$  is dielectric, while medium  $j+1$  is metallic. At their interfaces, the magnetic field  $H_y$  is continuous, as is  $E_x$ , which can be calculated using Eq. (8). A supplementary condition inside the metal is given by Eq. (18). A straightforward calculation shows that this leads to the following conditions on the coefficients:

$$A_j^- + B_j^- = A_{j+1}^+ + B_{j+1}^+, \quad (28)$$

$$\frac{k_z^j}{\epsilon_j} (A_j^- - B_j^-) = \frac{ik_z^{j+1}}{\epsilon_{j+1}} (A_{j+1}^+ - B_{j+1}^+) + C_{j+1}^+ + D_{j+1}^+, \quad (29)$$

$$D_{j+1}^+ - C_{j+1}^+ = i\Omega (A_{j+1}^+ + B_{j+1}^+). \quad (30)$$

Rearranging these equations, a scattering matrix  $S_{dm}$  for the dielectric-metal interface can be written so that

$$\begin{bmatrix} A_j^- \\ B_{j+1}^+ \\ D_{j+1}^+ \end{bmatrix} = S_{dm} \begin{bmatrix} B_j^- \\ A_{j+1}^+ \\ C_{j+1}^+ \end{bmatrix}, \quad (31)$$

where  $S_{dm}$  is equal to

$$\alpha \begin{bmatrix} \frac{k_z^j}{\epsilon_j} - \frac{ik_t^{j+1}}{\epsilon_{j+1}} + i\Omega & 2\frac{ik_t^{j+1}}{\epsilon_{j+1}} & 2 \\ 2\frac{k_z^j}{\epsilon_j} & \frac{ik_t^{j+1}}{\epsilon_{j+1}} - \frac{k_z^j}{\epsilon_j} + i\Omega & 2 \\ 2i\Omega\frac{k_z^j}{\epsilon_j} & 2i\Omega\frac{ik_t^{j+1}}{\epsilon_{j+1}} & \frac{k_z^j}{\epsilon_j} + \frac{ik_t^{j+1}}{\epsilon_{j+1}} + i\Omega \end{bmatrix}, \quad (32)$$

and

$$\alpha = \frac{1}{\frac{k_z^j}{\epsilon_j} + \frac{ik_t^{j+1}}{\epsilon_{j+1}} - i\Omega}. \quad (33)$$

### C. Metal to Dielectric Scattering Matrix

Similarly, at the interface between a metal (upper layer  $j$ ) and a dielectric (lower layer  $j+1$ ), the boundary conditions lead to the following equations:

$$A_j^- + B_j^- = A_{j+1}^+ + B_{j+1}^+, \quad (34)$$

$$\frac{ik_t^j}{\epsilon_j}(A_j^- - B_j^-) + C_j^- + D_j^- = \frac{k_z^{j+1}}{\epsilon_{j+1}}(A_{j+1}^+ - B_{j+1}^+), \quad (35)$$

$$D_j^- - C_j^- = i\Omega(A_j^- + B_j^-), \quad (36)$$

which, once they have been re-arranged, become a matrix  $S_{md}$ ,

$$\begin{bmatrix} A_j^- \\ C_j^- \\ B_{j+1}^+ \end{bmatrix} = S_{md} \begin{bmatrix} B_j^- \\ D_j^- \\ A_{j+1}^+ \end{bmatrix}, \quad (37)$$

where  $S_{dm}$  can be written

$$\alpha' \begin{bmatrix} \frac{ik_t^j}{\epsilon_j} - \frac{k_z^{j+1}}{\epsilon_{j+1}} + i\Omega & -2 & 2\frac{k_z^{j+1}}{\epsilon_{j+1}} \\ -2i\Omega\frac{ik_t^j}{\epsilon_j} & \frac{ik_t^j}{\epsilon_j} + \frac{k_z^{j+1}}{\epsilon_{j+1}} + i\Omega & -2i\Omega\frac{k_z^{j+1}}{\epsilon_{j+1}} \\ 2b_i^- & -2 & \frac{k_z^{j+1}}{\epsilon_{j+1}} - \frac{ik_t^j}{\epsilon_j} + i\Omega \end{bmatrix}, \quad (38)$$

with

$$\alpha' = \frac{1}{\frac{ik_t^j}{\epsilon_j} + \frac{k_z^{j+1}}{\epsilon_{j+1}} - i\Omega}. \quad (39)$$

### D. Cascading Method

Now that scattering matrices have been defined for all kinds of interfaces, they have to be combined through a cascading method. Here, the scattering matrices are all square matrices, but they may have more than two lines, so that the usual cascading algorithm cannot be used. Instead, one has to rely on the cascading algorithm that is usually employed for Fourier Modal Methods [70,71]. When trying to combine a scattering matrix  $\mathbf{S}$  so that

$$\begin{bmatrix} \mathbf{A} \\ \mathbf{B} \end{bmatrix} = \begin{bmatrix} \mathbf{S}_{11} & \mathbf{S}_{12} \\ \mathbf{S}_{21} & \mathbf{S}_{22} \end{bmatrix} \begin{bmatrix} \mathbf{C} \\ \mathbf{D} \end{bmatrix}, \quad (40)$$

with a scattering matrix  $\mathbf{U}$  such that

$$\begin{bmatrix} \mathbf{D} \\ \mathbf{E} \end{bmatrix} = \begin{bmatrix} \mathbf{U}_{11} & \mathbf{U}_{12} \\ \mathbf{U}_{21} & \mathbf{U}_{22} \end{bmatrix} \begin{bmatrix} \mathbf{B} \\ \mathbf{F} \end{bmatrix}, \quad (41)$$

to obtain a matrix  $\mathbf{T}$  so that

$$\begin{bmatrix} \mathbf{A} \\ \mathbf{E} \end{bmatrix} = \begin{bmatrix} \mathbf{T}_{11} & \mathbf{T}_{12} \\ \mathbf{T}_{21} & \mathbf{T}_{22} \end{bmatrix} \begin{bmatrix} \mathbf{C} \\ \mathbf{F} \end{bmatrix}. \quad (42)$$

Then  $\mathbf{T}$  is given by

$$\mathbf{T}_{11} = \mathbf{S}_{11} + \mathbf{S}_{12}(\mathbf{1} - \mathbf{S}_{11}\mathbf{U}_{22})^{-1}\mathbf{U}_{11}\mathbf{S}_{21}, \quad (43)$$

$$\mathbf{T}_{12} = \mathbf{S}_{12}(\mathbf{1} - \mathbf{S}_{11}\mathbf{U}_{22})^{-1}\mathbf{U}_{12}, \quad (44)$$

$$\mathbf{T}_{21} = \mathbf{U}_{21}(\mathbf{1} - \mathbf{S}_{22}\mathbf{U}_{11})^{-1}\mathbf{S}_{21}, \quad (45)$$

$$\mathbf{T}_{22} = \mathbf{U}_{22} + \mathbf{U}_{21}(\mathbf{1} - \mathbf{S}_{22}\mathbf{U}_{11})^{-1}\mathbf{S}_{22}\mathbf{U}_{12}. \quad (46)$$

This method can be applied here, although the  $\mathbf{U}_{ij}$  is generally not square. Here,  $\mathbf{A}$ ,  $\mathbf{B}$ ,  $\mathbf{C}$ ,  $\mathbf{D}$ ,  $\mathbf{E}$  and  $\mathbf{F}$  may represent vectors as  $\begin{bmatrix} A_j^\pm \\ C_j^\pm \end{bmatrix}$ ,  $\begin{bmatrix} B_j^\pm \\ D_j^\pm \end{bmatrix}$ , or simply  $[A_j^\pm]$  or  $[B_j^\pm]$ , depending on the scattering matrix. Each time a cascade is needed, there is, however, no ambiguity on how to choose the vectors, given the size of the matrices that have to be cascaded.

To compute the field inside the layers, beyond the reflection and transmission coefficients of the whole structure, it is necessary to compute the vectors that are eliminated during the cascading process. They can be obtained through the following relations:

$$\begin{bmatrix} \mathbf{B} \\ \mathbf{D} \end{bmatrix} = \begin{bmatrix} (\mathbf{1} - \mathbf{S}_{22}\mathbf{U}_{11})^{-1}\mathbf{S}_{21} & (\mathbf{1} - \mathbf{S}_{22}\mathbf{U}_{11})^{-1}\mathbf{S}_{22}\mathbf{U}_{12} \\ (\mathbf{1} - \mathbf{S}_{11}\mathbf{U}_{22})^{-1}\mathbf{U}_{11}\mathbf{S}_{21} & (\mathbf{1} - \mathbf{S}_{11}\mathbf{U}_{22})^{-1}\mathbf{U}_{12} \end{bmatrix} \begin{bmatrix} \mathbf{C} \\ \mathbf{F} \end{bmatrix}. \quad (47)$$

Finally, once all the  $A_j^\pm$ ,  $B_j^\pm$  have been obtained using the previous method, the most stable way to compute the magnetic field (but this is true for any other field) is to use the following hybrid expression inside a layer,

$$H_y = (A_j^- e^{ik_z^j(z-z_{j+1})} + B_j^+ e^{-ik_z^j(z-z_j)})e^{i(k_x x - \omega t)}, \quad (48)$$

with  $k_z^j = ik_t^j$  in the case of a metallic layer, to ensure the exponentials have a modulus as small as possible.

## 4. SIMULATION RESULTS

The purpose of this section is to put the numerical method we have devised to a test. We have implemented the above scattering matrix algorithm, basing it on a code we have previously released [59], and that has been used previously to simulate the propagation of light beams in finite metallo-dielectric layers [19,67]. The structure can be illuminated with a Gaussian beam, which can be considered as a superposition of plane waves. In that case, the field inside each layer is computed as a superposition of the fields associated with each plane wave. The amplitude of each plane wave is given here by

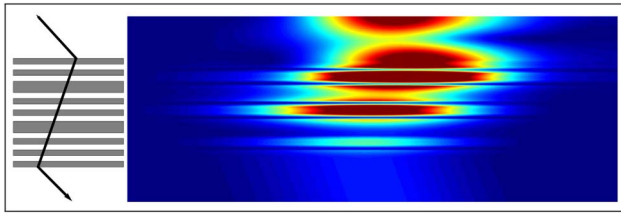
$$A(k_x) = \frac{w}{2\sqrt{\pi}} e^{-\frac{w^2}{4}(k_x - k_{x,0})^2} e^{-k_x x_0}, \quad (49)$$

where  $w$  is the waist of the beam, its characteristic width;  $x_0$  is the center of the beam; and  $k_{x,0} = nk_0 \sin \theta$ ,  $\theta$  being the incidence angle and  $x_0$  the location of the center of the beam.

When the waist is made very small (typically a tenth of the wavelength), the source can be considered as almost punctual. This is the kind of source we are considering to assess the sub-wavelength imaging capabilities of the designs we study here.

### A. Impact of Nonlocality on a Slab of $-1$ Index Metamaterial

We first consider the structure known to behave as a  $-1$  index medium [66] which has been recently fabricated [8]. The structure we study is finite, and the incoming medium is air.



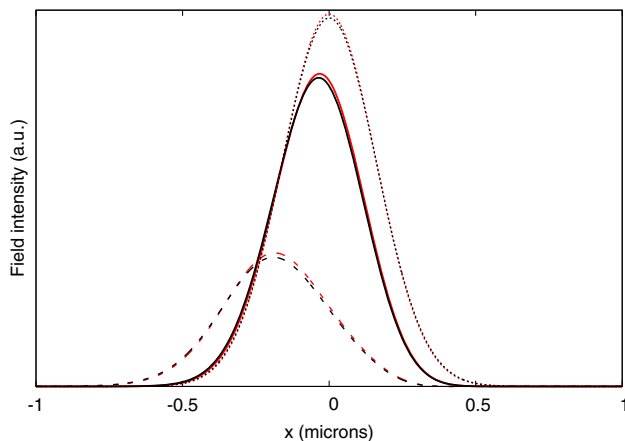
**Fig. 2.** Propagation of an incident Gaussian beam with a waist  $w = \lambda$  through a  $-1$  index lens [8], showing the negative refraction phenomenon, illustrated on the left. The modulus of the magnetic field is plotted on the right. The incident medium is air.

Figure 2 shows the setup and the propagation of a beam inside the structure.

This lens operation wavelength is of 363.8 nm, in the close UV range. In that range, the plasmonic effects are actually much higher [72]. They are usually linked to the Poynting vector inside the metal, which is roughly proportional to  $\frac{1}{\epsilon}$ , a factor that becomes important when the permittivity is negative but small. However, it is however not possible to consider a much shorter wavelength because the titanium oxide then becomes much more absorbent. This is what makes this close UV range so interesting for building flat lenses, and this is a range for which the nonlocal effects are much more likely to be noticeable, too. We have simulated what happens when the structure is illuminated with a Gaussian beam with a non-normal incidence, an experiment that has been made to study the negative refraction. A typical result is shown in Fig. 2. To compare local and nonlocal simulations, in Fig. 3, we have plotted different beam profile, for various incidence angles. There is very little difference between the two. This can be related to the fact that nonlocal effects can be seen for large wave vectors that are not concerned by this kind of experiment.

### B. Impact of the Channeling Regime

Keeping the same materials and operation wavelength, it is possible to find a structure in the channeling regime, i.e., presenting a flat dispersion curve according to the local theory [13]. In



**Fig. 3.** Transmitted beam for different incidence angles (dotted line, normal incidence; solid line, 20°; dashed line, 40°) for the local (black) and the nonlocal (red) computation in the case of the  $-1$  lens [8]. The waist of the incident beam is  $w = \lambda$ .

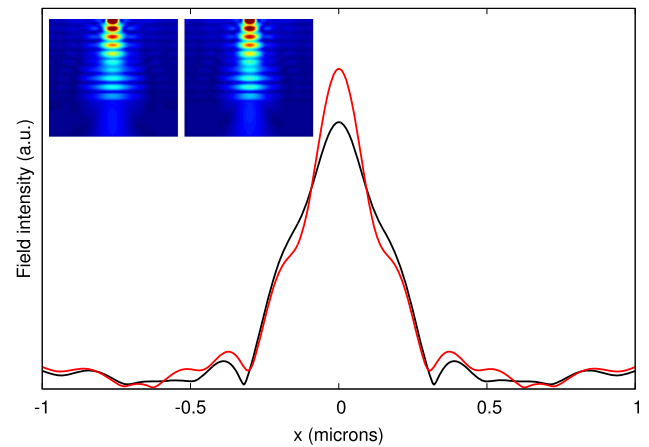


**Fig. 4.** Profile of the outgoing beam (magnetic field) for the local (black) and nonlocal (red) computation [case (1)]. The field profile is computed at the very edge of the lens. Inset: local (left) and nonlocal (right) corresponding field maps for the magnetic field. The incoming medium (not shown here) is air.

such a medium, all the waves (whether they are evanescent in the outside medium or not) propagate, and they do it in the same direction. As long as the ratio  $\frac{b_d}{b_m}$  is equal to the ratio  $|\frac{\epsilon_d}{\epsilon_m}| \simeq 4.2$ , and the overall period stays small with respect to the wavelength, we can consider that we are in the channeling regime. The following two cases are considered here: (1) a 10-period structure with a 10 nm metallic layer and a 42 nm dielectric layer, and (2) a 25-period structure with a 4 nm metallic layer and a 16.8 nm thick dielectric layer. Both structures begin and terminate with a metallic layer so that their respective thicknesses are 530 and 524 nm. The structure is illuminated with a Gaussian beam (normal incidence, wavelength of  $\lambda = 363.8$  nm, waist of 0.1 nm, and focused on the entrance of the structure). It should be underlined that what we call a Gaussian beam contains evanescent waves, so that it is actually almost a point source. The results of the computation are

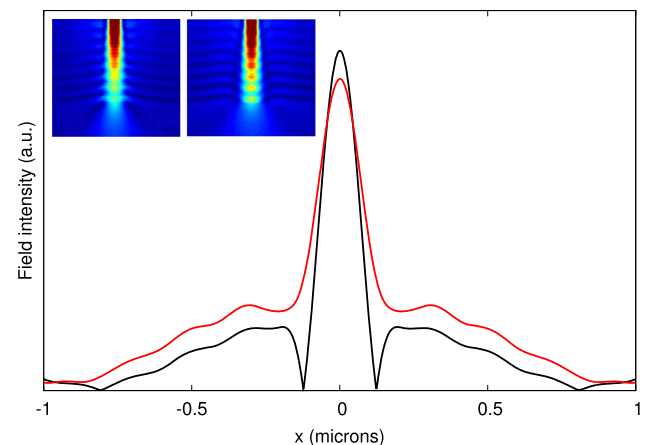


**Fig. 5.** Profile of the outgoing beam for the local (black) and nonlocal (red) computation [case (2)]. The field profile is computed at the very edge of the lens. Inset: local (left) and nonlocal (right) corresponding field maps for the magnetic field. The incoming medium (not shown here) is air.

shown in Fig. 4 for the first case with 10 nm thick metallic layers and in Fig. 5 for the second case with thinner layers.

An important point is that the predictions of the local theory are significantly different from the nonlocal one when it comes to the profile of the outgoing beam. This means that nonlocality can definitely not be ignored, when the whole purpose of the structure is to make an image of a source with subwavelength resolution. Another interesting feature is the higher transmission when nonlocality is considered. For both situations described above, we have computed the total Poynting vector flux in the vertical direction. This flux is 6.6% higher for the 10 nm thick metallic layers, and 5.1% higher in the case of 4 nm thick metallic layers. The difference is noticeable and can be attributed to the fact that the bulk plasmon acts for light as a supplementary channel through the metallic layers.

## 5. CONCLUSION

We have presented here numerical tools that allow us to take nonlocality in metals into account when simulating the propagation of a plane wave or of a beam in a metallo-dielectric multilayer. These tools, relying essentially on analytical calculations, are meant to be as accurate as possible, through the use of accurate material characteristics [60] and boundary conditions that can be considered *conservative* [26] compared to other implementations of the hydrodynamic model. The formulas presented here are easy to adapt for different descriptions of the metal and different boundary conditions, so that previous results can be retrieved and checked using the present work. Furthermore, if the hydrodynamic model needs further tuning to match future experiments, the present formalism should be very easy to adapt. Finally, we have made the codes we have written freely available [73].

We have used these tools to assess the impact of nonlocality on realistic metallo-dielectric structures, presenting a negative refractive index, and on the channeling regime. Our conclusions are that, for a negative index around  $-1$ , the impact of nonlocality should be expected to be negligible. For higher absolute values of the refractive index that are required to reach subwavelength resolution, and, especially in the channeling regime, the effect of nonlocality cannot be ignored. We underline that, even small effects such as the small change in the effective index because of nonlocality, will have an impact on the operation of flat lenses, especially when they are able to reach super-resolution [19]. In that case, the propagation of high wave vector waves is actually responsible for the subwavelength resolution [13,15]. Thus, the structure has to be finely optimized [65], and there is little doubt that nonlocal effects should be taken into account. The tools we have provided here should help to finely simulate the optical behavior of such structures.

We hope that the present work will make it easy for the community to assess the impact of nonlocality thoroughly and to take it accurately into account, to design structures or experiments based on metallo-dielectric multilayers.

**Funding.** Agence Nationale de la Recherche (ANR) (ANR-13-JS10-0003).

## REFERENCES

1. M. Scalora, M. Bloemer, A. Pethel, J. Dowling, C. Bowden, and A. Manka, "Transparent, metallo-dielectric, one-dimensional, photonic band-gap structures," *J. Appl. Phys.* **83**, 2377–2383 (1998).
2. W. Cai, D. A. Genov, and V. M. Shalae, "Superlens based on metallo-dielectric composites," *Phys. Rev. B* **72**, 193101 (2005).
3. M. Scalora, G. D'Aguanno, N. Mattiucci, M. J. Bloemer, D. de Ceglia, M. Centini, A. Mandatori, C. Sibilia, N. Akozbek, M. G. Cappeddu, M. Fowler, and J. W. Haus, "Negative refraction and sub-wavelength focusing in the visible range using transparent metallo-dielectric stacks," *Opt. Express* **15**, 508–523 (2007).
4. A. J. Hoffman, L. Alekseyev, S. S. Howard, K. J. Franz, D. Wasserman, V. A. Podolskiy, E. E. Narimanov, D. L. Sivco, and C. Gmachl, "Negative refraction in semiconductor metamaterials," *Nat. Mater.* **6**, 946–950 (2007).
5. Z. Liu, H. Lee, Y. Xiong, C. Sun, and X. Zhang, "Far-field optical hyperlens magnifying sub-diffraction-limited objects," *Science* **315**, 1686 (2007).
6. M. Noginov, Y. A. Barnakov, G. Zhu, T. Tumkur, H. Li, and E. Narimanov, "Bulk photonic metamaterial with hyperbolic dispersion," *Appl. Phys. Lett.* **94**, 151105 (2009).
7. C. Cortes, W. Newman, S. Molesky, and Z. Jacob, "Quantum nanophotonics using hyperbolic metamaterials," *J. Opt.* **14**, 063001 (2012).
8. T. Xu, A. Agrawal, M. Abashin, K. J. Chau, and H. J. Lezec, "All-angle negative refraction and active flat lensing of ultraviolet light," *Nature* **497**, 470–474 (2013).
9. S.-A. Biehs, M. Tschikin, and P. Ben-Abdallah, "Hyperbolic metamaterials as an analog of a blackbody in the near field," *Phys. Rev. Lett.* **109**, 104301 (2012).
10. Y. Guo, C. L. Cortes, S. Molesky, and Z. Jacob, "Broadband super-Planckian thermal emission from hyperbolic metamaterials," *Appl. Phys. Lett.* **101**, 131106 (2012).
11. E. Narimanov and I. Smolyaninov, "Beyond Stefan-Boltzmann law: thermal hyper-conductivity," in *Quantum Electronics and Laser Science Conference* (Optical Society of America, 2012), paper QM2E-1.
12. N. Fang, H. Lee, C. Sun, and X. Zhang, "Sub-diffraction-limited optical imaging with a silver superlens," *Science* **308**, 534–537 (2005).
13. P. A. Belov, C. R. Simovski, and P. Ikonen, "Canalization of subwavelength images by electromagnetic crystals," *Phys. Rev. B* **71**, 193105 (2005).
14. Z. Jacob, L. V. Alekseyev, and E. Narimanov, "Optical hyperlens: far-field imaging beyond the diffraction limit," *Opt. Express* **14**, 8247–8256 (2006).
15. P. A. Belov and Y. Hao, "Subwavelength imaging at optical frequencies using a transmission device formed by a periodic layered metallo-dielectric structure operating in the canalization regime," *Phys. Rev. B* **73**, 113110 (2006).
16. I. I. Smolyaninov, Y.-J. Hung, and C. C. Davis, "Magnifying superlens in the visible frequency range," *Science* **315**, 1699–1701 (2007).
17. X. Zhang and Z. Liu, "Superlenses to overcome the diffraction limit," *Nat. Mater.* **7**, 435–441 (2008).
18. N. Mattiucci, G. D'Aguanno, M. Scalora, M. Bloemer, and C. Sibilia, "Transmission function properties for multi-layered structures: application to super-resolution," *Opt. Express* **17**, 17517–17529 (2009).
19. J. Bénédicto, E. Centeno, and A. Moreau, "Lens equation for flat lenses made with hyperbolic metamaterials," *Opt. Lett.* **37**, 4786–4788 (2012).
20. C. Ciraci, R. Hill, J. Mock, Y. Urzhumov, A. Fernández-Domínguez, S. Maier, J. Pendry, A. Chilkoti, and D. Smith, "Probing the ultimate limits of plasmonic enhancement," *Science* **337**, 1072–1074 (2012).
21. A. D. Boardman, *Electromagnetic Surface Modes* (Wiley, 1982).
22. F. Frostmann and R. R. Gerhardt, *Metal Optics Near the Plasma Frequency*, Vol. **109** (Springer-Verlag, 1986).
23. R. Ruppin, "Non-local optics of the near field lens," *J. Phys.* **17**, 1803–1810 (2005).
24. R. Ruppin and K. Kempa, "Nonlocal effects on the imaging properties of a silver superlens," *Phys. Rev. B* **72**, 153105 (2005).

25. W. Yan, N. Asger Mortensen, and M. Wubs, "Hyperbolic metamaterial lens with hydrodynamic nonlocal response," *Opt. Express* **21**, 15026–15036 (2013).
26. A. Moreau, C. Ciraci, and D. R. Smith, "Impact of nonlocal response on metalodielectric multilayers and optical patch antennas," *Phys. Rev. B* **87**, 045401 (2013).
27. W. L. Mochán, M. del Castillo-Mussot, and R. G. Barrera, "Effect of plasma waves on the optical properties of metal-insulator superlattices," *Phys. Rev. B* **35**, 1088–1098 (1987).
28. W. Yan, M. Wubs, and N. A. Mortensen, "Hyperbolic metamaterials: Nonlocal response regularizes broadband supersingularity," *Phys. Rev. B* **86**, 205429 (2012).
29. M. Scalora, M. A. Vincenti, D. de Ceglia, V. Roppo, M. Centini, N. Akozbek, and M. J. Bloemer, "Second- and third-harmonic generation in metal-based structures," *Phys. Rev. A* **82**, 043828 (2010).
30. N. Crouseilles, P. A. Hervieux, and G. Manfredi, "Quantum hydrodynamic model for the nonlinear electron dynamics in thin metal films," *Phys. Rev. B* **78**, 155412 (2008).
31. K. Kliewer and R. Fuchs, "Anomalous skin effect for specular electron scattering and optical experiments at non-normal angles of incidence," *Phys. Rev.* **172**, 607–624 (1968).
32. A. R. Melnyk and M. J. Harrison, "Theory of optical excitation of plasmons in metals," *Phys. Rev. B* **2**, 835–850 (1970).
33. R. Fuchs and R. G. Barrera, "Dynamical response of a dipole near the surface of a nonlocal metal," *Phys. Rev. B* **24**, 2940–2950 (1981).
34. R. R. Gerhardts and K. Kempa, "Microscopic generalization of the Kliewer-Fuchs theory of surface electromagnetic fields," *Phys. Rev. B* **30**, 5704–5720 (1984).
35. G. S. Agarwal and S. V. O'Neil, "Effect of hydrodynamic dispersion of the metal on surface plasmons and surface-enhanced phenomena in spherical geometries," *Phys. Rev. B* **28**, 487–493 (1983).
36. R. Fuchs and F. Claro, "Multipolar response of small metallic spheres: Nonlocal theory," *Phys. Rev. B* **35**, 3722–3727 (1987).
37. P. Halevi, "Hydrodynamic model for the degenerate free-electron gas: Generalization to arbitrary frequencies," *Phys. Rev. B* **51**, 7497–7499 (1995).
38. G. W. Ford and W. Weber, "Electromagnetic interactions of molecules with metal surfaces," *Phys. Rep.* **113**, 195–287 (1984).
39. P.-O. Chapuis, S. Volz, C. Henkel, K. Joulain, and J.-J. Greffet, "Effects of spatial dispersion in near-field radiative heat transfer between two parallel metallic surfaces," *Phys. Rev. B* **77**, 035431 (2008).
40. P. Feibelman, "Surface electromagnetic fields," *Prog. Surf. Sci.* **12**, 287–407 (1982).
41. A. Liebsch, "Dynamical screening at simple-metal surfaces," *Phys. Rev. B* **36**, 7378–7388 (1987).
42. A. Liebsch and W. L. Schaich, "Influence of a polarizable medium on the nonlocal optical response of a metal surface," *Phys. Rev. B* **52**, 14219–14234 (1995).
43. K. J. Savage, M. M. Hawkeye, R. Esteban, A. G. Borisov, J. Aizpurua, and J. J. Baumberg, "Revealing the quantum regime in tunneling plasmonics," *Nature* **491**, 574–577 (2012).
44. T. Teperik, P. Nordlander, J. Aizpurua, and A. Borisov, "Robust subnanometric plasmon ruler by rescaling of the nonlocal optical response," *Phys. Rev. Lett.* **110**, 263901 (2013).
45. R. Esteban, A. G. Borisov, P. Nordlander, and J. Aizpurua, "Bridging quantum and classical plasmonics with a quantum-corrected model," *Nat. Commun.* **3**, 825 (2012).
46. C. Ciraci, J. B. Pendry, and D. R. Smith, "Hydrodynamic model for plasmonics: A macroscopic approach to a microscopic problem," *ChemPhysChem* **14**, 1109–1116 (2013).
47. Y. Luo, A. Fernandez-Dominguez, A. Wiener, S. A. Maier, and J. Pendry, "Surface plasmons and nonlocality: a simple model," *Phys. Rev. Lett.* **111**, 093901 (2013).
48. C. David, N. A. Mortensen, and J. Christensen, "Perfect imaging, epsilon-near zero phenomena and waveguiding in the scope of nonlocal effects," *Sci. Rep.* **3**, 2526 (2013).
49. J. A. Scholl, A. L. Koh, and J. A. Dionne, "Quantum plasmon resonances of individual metallic nanoparticles," *Nature* **483**, 421–427 (2012).
50. J. A. Scholl, A. Garca-Etxarri, A. L. Koh, and J. A. Dionne, "Observation of quantum tunneling between two plasmonic nanoparticles," *Nano Lett.* **13**, 564–569 (2013).
51. A. I. Fernandez-Dominguez, A. Wiener, F. J. Garcia-Vidal, S. A. Maier, and J. B. Pendry, "Transformation-optics description of nonlocal effects in plasmonic nanostructures," *Phys. Rev. Lett.* **108**, 106802 (2012).
52. C. Ciraci, Y. Urzhumov, and D. R. Smith, "Effects of classical nonlocality on the optical response of three-dimensional plasmonic nanodimers," *J. Opt. Soc. Am. B* **30**, 2731–2736 (2013).
53. A. Wiener, A. I. Fernández-Dominguez, A. P. Horsfield, J. B. Pendry, and S. A. Maier, "Nonlocal effects in the nanofocusing performance of plasmonic tips," *Nano Lett.* **12**, 3308–3314 (2012).
54. A. Fernandez-Dominguez, P. Zhang, Y. Luo, S. Maier, F. Garcia-Vidal, and J. Pendry, "Transformation-optics insight into nonlocal effects in separated nanowires," *Phys. Rev. B* **86**, 241110 (2012).
55. S. Raza, T. Christensen, M. Wubs, S. Bozhevolnyi, and N. Mortensen, "Nonlocal response in thin-film waveguides: Loss versus nonlocality and breaking of complementarity," *Phys. Rev. B* **88**, 115401 (2013).
56. A. Moreau, C. Ciraci, J. J. Mock, R. T. Hill, Q. Wang, B. J. Wiley, A. Chilkoti, and D. R. Smith, "Controlled-reflectance surfaces with film-coupled colloidal nanoantennas," *Nature* **492**, 86–89 (2012).
57. S. Raza, G. Toscano, A. P. Jauho, M. Wubs, and N. A. Mortensen, "Unusual resonances in nanoplasmonic structures due to nonlocal response," *Phys. Rev. B* **84**, 121412 (2011).
58. A. Moreau and D. Felbacq, "Leaky modes of a left-handed slab," *J. Eur. Opt. Soc. Rapid Publ.* **3**, 08032 (2008).
59. F. Krayzel, R. Polles, A. Moreau, M. Mihailovic, and G. Granet, "Simulation and analysis of exotic non-specular phenomena," *J. Eur. Opt. Soc. Rapid Publ.* **5**, 10025 (2010).
60. A. D. Rakic, A. B. Djurišić, J. M. Elazar, and M. L. Majewski, "Optical properties of metallic films for vertical-cavity optoelectronic devices," *Appl. Opt.* **37**, 5271–5283 (1998).
61. W. L. Mochán and M. del CastilloMussot, "Optics of multilayered conducting systems: Normal modes of periodic superlattices," *Phys. Rev. B* **37**, 6763–6771 (1988).
62. D. Smith and D. Schurig, "Electromagnetic wave propagation in media with indefinite permittivity and permeability tensors," *Phys. Rev. Lett.* **90**, 077405 (2003).
63. D. R. Smith, P. Kolinko, and D. Schurig, "Negative refraction in indefinite media," *J. Opt. Soc. Am. B* **21**, 1032–1043 (2004).
64. M. Bloemer, G. D'Aguanno, N. Mattiucci, M. Scalora, and N. Akozbek, "Broadband super-resolving lens with high transparency in the visible range," *Appl. Phys. Lett.* **90**, 174113 (2007).
65. J. Bénédicte, E. Centeno, R. Pollès, and A. Moreau, "Ultimate resolution of indefinite metamaterial flat lenses," *Phys. Rev. B* **88**, 245138 (2013).
66. E. Verhagen, R. de Waele, L. Kuipers, and A. Polman, "Three-dimensional negative index of refraction at optical frequencies by coupling plasmonic waveguides," *Phys. Rev. Lett.* **105**, 223901 (2010).
67. J. Benédicte, R. Pollès, A. Moreau, and E. Centeno, "Large negative lateral shifts due to negative refraction," *Opt. Lett.* **36**, 2539–2541 (2011).
68. <http://www.comsol.com>.
69. G. Toscano, S. Raza, A.-P. Jauho, N. A. Mortensen, and M. Wubs, "Modified field enhancement and extinction by plasmonic nanowire dimers due to nonlocal response," *Opt. Express* **20**, 4176–4188 (2012).
70. P. Lalanne and G. M. Morris, "Highly improved convergence of the coupled-wave method for tm polarization," *J. Opt. Soc. Am. A* **13**, 779–784 (1996).
71. G. Granet and B. Guizal, "Efficient implementation of the coupled-wave method for metallic lamellar gratings in tm polarization," *J. Opt. Soc. Am. A* **13**, 1019–1023 (1996).
72. J. Benédicte, A. Moreau, R. Pollès, and E. Centeno, "Comment on 'negative refraction in 1d photonic crystals' [Solid State Commun. 147, 157-160 (2008)]," *Solid State Commun.* **151**, 354–355 (2011).
73. [http://elma.univ-bpclermont.fr/moreau/pgp/index\\_en.html](http://elma.univ-bpclermont.fr/moreau/pgp/index_en.html).